

EXCLUSIVE BARYON-ANTIBARYON PRODUCTION IN $\gamma\gamma$ COLLISIONS AT e^+e^- COLLIDERS

T. BARILLARI

*Max-Planck-Inst. für Physik,
Werner-Heisenberg-Institut,
Föhringer Ring 6,
D-80805 München, Germany
E-mail: barilla@mppmu.mpg.de*

The exclusive production of baryon-antibaryon pairs in the collisions of two quasi-real photons has been studied using different detectors at e^+e^- colliders. Results are presented for $\gamma\gamma \rightarrow p\bar{p}$, $\gamma\gamma \rightarrow \Lambda\bar{\Lambda}$, and $\gamma\gamma \rightarrow \Sigma^0\bar{\Sigma}^0$ final states. The cross-section measurements are compared with all the existing experimental data and with the analytic calculations based on the three-quark model, on the quark-diquark model, and on the handbag model.

1. Introduction

The exclusive production of baryon-antibaryon ($B\bar{B}$) pairs in the collision of two quasi-real photons can be used to test predictions of QCD. At e^+e^- colliders the photons are emitted by the beam electrons^a and the $B\bar{B}$ pairs are produced in the process $e^+e^- \rightarrow e^+e^-\gamma\gamma \rightarrow e^+e^-\bar{B}\bar{B}$.

The application of QCD to exclusive photon-photon reactions is based on the work of Brodsky and Lepage¹. According to their formalism the process is factorized into a non-perturbative part, which is the hadronic wave function of the final state, and a perturbative part. Calculations based on this ansatz^{2,3} yields e.g. $e^+e^- \rightarrow e^+e^-\gamma\gamma \rightarrow e^+e^-\bar{p}\bar{p}$ cross-sections about one order of magnitude smaller than the existing experimental results^{4,5,6,7,8,9}, for $p\bar{p}$ centre-of-mass energies W greater than 2.5 GeV.

Recent studies¹⁰ have extended the systematic investigation of hard exclusive reactions within the quark-diquark model to photon-photon processes^{11,12}. In addition, the handbag contribution¹³ has been recently proposed to describe the photon-photon annihilation into baryon-antibaryon pairs at large momentum transfer.

^aIn this paper positrons are also referred to as electrons.

In this paper, all the existing measurements of the cross-sections for the exclusive $e^+e^- \rightarrow e^+e^-B\bar{B}$ processes are presented. In particular, results for $\gamma\gamma \rightarrow p\bar{p}$, $\gamma\gamma \rightarrow \Lambda\bar{\Lambda}$, and $\gamma\gamma \rightarrow \Sigma^0\bar{\Sigma}^0$ final states are reported. These cross-section measurements are compared with the analytic calculations based on the three-quark model, on the quark-diquark model, and on the handbag model.

2. The $\gamma\gamma \rightarrow p\bar{p}$ cross-section measurements

The differential cross-section for the process $e^+e^- \rightarrow e^+e^-p\bar{p}$ is given by

$$\frac{d^2\sigma(e^+e^- \rightarrow e^+e^-p\bar{p})}{dW d|\cos\theta^*|} = \frac{N_{ev}(W, |\cos\theta^*|)}{\mathcal{L}_{e^+e^-} \varepsilon_{TRIG} \varepsilon_{DET}(W, |\cos\theta^*|) \Delta W \Delta |\cos\theta^*|}$$

where N_{ev} is the number of events selected in each $(W, |\cos\theta^*|)$ bin, ε_{TRIG} is the trigger efficiency, ε_{DET} is the detection efficiency, $\mathcal{L}_{e^+e^-}$ is the measured integrated luminosity, and ΔW and $\Delta |\cos\theta^*|$ are the bin widths in W and in $|\cos\theta^*|$.

The total cross-section $\sigma(\gamma\gamma \rightarrow p\bar{p})$ for a given value of $\sqrt{s_{ee}}$ is derived from the differential cross-section $d\sigma(e^+e^- \rightarrow e^+e^-p\bar{p})/dW$ by using the luminosity function $d\mathcal{L}_{\gamma\gamma}/dW$ ¹⁴.

The resulting differential cross-sections for the process $\gamma\gamma \rightarrow p\bar{p}$ in bins of W and $|\cos\theta^*|$ are then summed over $|\cos\theta^*|$ to obtain the total cross-section as a function of W for $|\cos\theta^*| < 0.6$.

Fig. 1a) shows the cross-section $\sigma(\gamma\gamma \rightarrow p\bar{p})$ measurements as a function of W for $|\cos\theta^*| < 0.6$ obtained by ARGUS⁴, CLEO⁵, VENUS⁶, OPAL⁷, L3⁸, and BELLE⁹. Some predictions based on the quark-diquark model^{10,11}, and the three-quark model² are also shown in this figure.

There is good agreement between the different experiments results for $W > 2.3\text{GeV}$. At $W < 2.3\text{GeV}$ the OPAL⁷ measurements agree with the ARGUS⁴ results, but both these measurements lie below the results obtained by CLEO⁵, VENUS⁶, L3⁸, and BELLE⁹.

Within the estimated theoretical uncertainties and for $W > 2.2\text{GeV}$ there is a good agreement between the L3⁸ and OPAL⁷ results and the quark-diquark model predictions^{10,11}. The three-quark model is excluded². At low W the BELLE⁹ results are above the quark-diquark model predictions. This measurement agrees with the quark-diquark model for $2.5\text{GeV} < W < 3.0\text{GeV}$, while at higher W a steeper fall of the BELLE⁹ cross-section is observed.

An important consequence of the pure quark hard scattering picture is the power law which follows from the dimensional counting rules^{15,16}. We expect that for asymptotically large W and fixed $|\cos\theta^*|$,

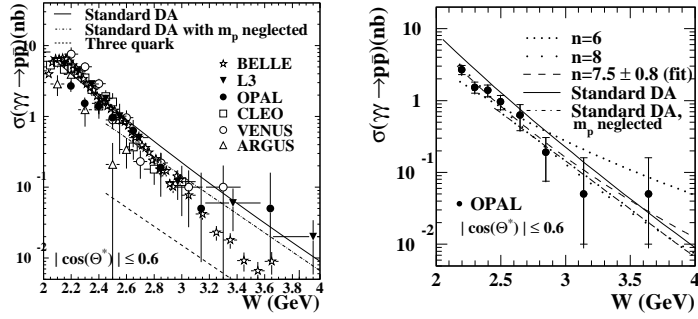


Figure 1. Cross-sections $\sigma(\gamma\gamma \rightarrow p\bar{p})$ as a function of W . The data and the theoretical predictions cover a range of $|\cos(\theta^*)| < 0.6$. a)(Left plot) The experimental data ^{4,5,6,7,8,9} are compared to the quark-diquark model prediction ¹⁰. The error bars include statistical and systematic uncertainties. b)(Right plot) The data are compared to the quark-diquark model predictions of ¹¹ (dash-dotted line), and of ¹⁰ (solid line), using the standard distribution amplitude (DA) with and without neglecting the mass m_p of the proton, and with the predictions of the power law with fixed and with fitted exponent n . The inner error bars are the statistical uncertainties and the outer error bars are the total uncertainties.

$d\sigma(\gamma\gamma \rightarrow p\bar{p})/dt \sim W^{2(2-n)}$ where $n = 8$ is the number of elementary fields and $t = -W^2/2(1 - |\cos(\theta^*)|)$. The introduction of diquarks modifies the power law by decreasing n to $n = 6$. This power law is compared to the OPAL data in Fig. 1b) with $\sigma(\gamma\gamma \rightarrow p\bar{p}) \sim W^{-2(n-3)}$ using three values of the exponent n : fixed values $n = 8$, $n = 6$, and the fitted value $n = 7.5 \pm 0.8$ obtained by taking into account statistical uncertainties only. More data covering a wider range of W would be required to determine the exponent n more precisely.

The measured differential cross-sections $d\sigma(\gamma\gamma \rightarrow p\bar{p})/d|\cos(\theta^*)|$ in different W ranges and for $|\cos(\theta^*)| < 0.6$ are shown in Fig. 2.

In the range $2.15 < W < 2.55$ GeV the OPAL ⁷ differential cross-section lies below the results reported by CLEO ⁵, VENUS ⁶, L3 ⁸, and BELLE ⁹ (Fig. 2a)). Since the CLEO measurements are given for the lower W range $2.0 < W < 2.5$ GeV, their results have been rescaled by a factor 0.635 which is the ratio of the two CLEO total cross-section measurements integrated over the W ranges $2.0 < W < 2.5$ GeV and $2.15 < W < 2.55$ GeV. This leads to a better agreement between the OPAL and CLEO measurements but the OPAL results are still consistently lower. The shapes of the $|\cos(\theta^*)|$ dependence of all measurements are consistent.

Fig. 2b) shows the differential cross-sections $d\sigma(\gamma\gamma \rightarrow p\bar{p})/d|\cos(\theta^*)|$ in the W range $2.5 < W < 3.0$ GeV obtained by CLEO ⁵, OPAL ⁷, L3 ⁸, and

BELLE ⁹ in similar W ranges, these differential cross-section have been normalized to the that averaged within $|\cos \theta^*| < 0.3$. The measurements are consistent within the uncertainties.

The comparison of the differential cross-section as a function of $|\cos \theta^*|$ for $2.55 < W < 2.95$ GeV with the calculation of ¹⁰ at $W = 2.8$ GeV for different distribution amplitudes (DA) is also shown in this figure together with pure quark model ² and the handbag model prediction ¹³. The shapes of the curves are consistent with those of the data. Fig. 2 shows that

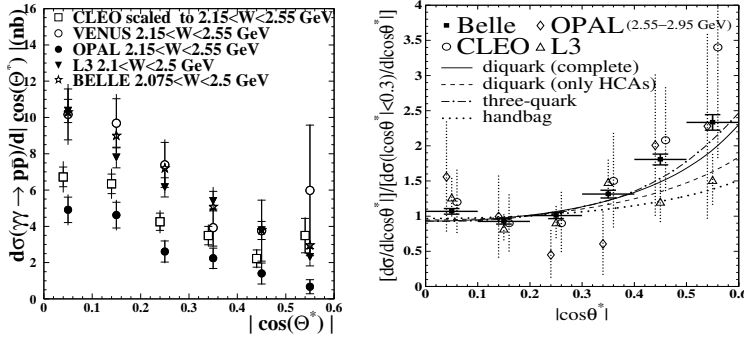


Figure 2. Differential cross-sections for $\gamma\gamma \rightarrow p\bar{p}$ as a function of $|\cos \theta^*|$ in different ranges of W ; a) (left plot) low range $2.15 < W < 2.55$ GeV, b) (right plot) higher range $2.5 < W < 3.0$ GeV. The inner error bars are the statistical uncertainties and the outer error bars are the total uncertainties.

the differential cross-section at low W decreases at large $|\cos \theta^*|$, while the opposite trend is observed in the higher W region. The transition point seems to occur at $W \approx 2.5$ GeV ⁹.

Another important consequence of the hard scattering picture is the hadron helicity conservation rule. For each exclusive reaction like $\gamma\gamma \rightarrow p\bar{p}$ the sum of the two initial helicities equals the sum of the two final ones. According to the simplification used in ¹¹, neglecting quark masses, quark and antiquark and hence proton and antiproton have to be in opposite helicity states. If the (anti) proton is considered as a point-like particle, simple QED rules determine the angular dependence of the unpolarized $\gamma\gamma \rightarrow p\bar{p}$ differential cross-section ¹⁷:

$$\frac{d\sigma(\gamma\gamma \rightarrow p\bar{p})}{d|\cos \theta^*|} \propto \frac{(1 + \cos^2 \theta^*)}{(1 - \cos^2 \theta^*)}. \quad (1)$$

This expression is compared to the OPAL ⁷ data in two W ranges, $2.55 < W < 2.95$ GeV (Fig. 3a) and $2.15 < W < 2.55$ GeV (Fig. 3b). The normalisation in each case is determined by the best fit to the data.

In the higher W range, the prediction (1) is in agreement with the data within the experimental uncertainties. In the lower W range this simple model does not describe the data. At low W soft processes such as meson exchange are expected to introduce other partial waves, so that the approximations leading to (1) become invalid.

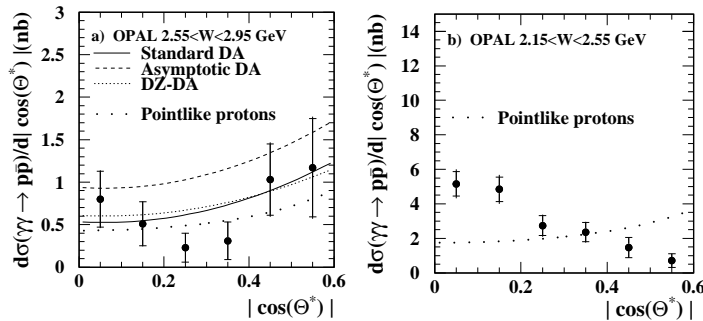


Figure 3. Measured differential cross-section, $d\sigma(\gamma\gamma \rightarrow p\bar{p})/d|\cos\theta^*|$, with statistical (inner bars) and total uncertainties (outer bars) for a) $2.55 < W < 2.95$ GeV and b) $2.15 < W < 2.55$ GeV. The data are compared with the point-like approximation for the proton (1) scaled to fit the data. The other curves show the pure quark model ², the diquark model of ¹¹ with the Dziembowski distribution amplitudes (DZ-DA), and the diquark model of ¹⁰ using standard and asymptotic distribution amplitudes.

3. The $\gamma\gamma \rightarrow \Lambda\bar{\Lambda}$ and $\gamma\gamma \rightarrow \Sigma^0\bar{\Sigma}^0$ cross-section measurements

The cross-sections $\sigma(\gamma\gamma \rightarrow \Lambda\bar{\Lambda})$ and $\sigma(\gamma\gamma \rightarrow \Sigma^0\bar{\Sigma}^0)$ in real photon collisions as a function of W and for $|\cos\theta^*| < 0.6$ can be extracted by deconvoluting the two-photon luminosity function and the form factor ¹⁴.

Fig. 4 compares the L3 ¹⁸ $\sigma(\gamma\gamma \rightarrow \Lambda\bar{\Lambda})$ measurement with that obtained by CLEO ¹⁹. For $W > 2.5$ GeV the two results are compatible inside the large experimental errors. The cross-section measurement obtained by CLEO at lower W values is steeper than the one obtained by L3. The L3 ¹⁸ data, fitted with a function of the form $\sigma \approx W^{-n}$, gives a value $n = 7.6 \pm 3.9$. In Fig. 4 the $\sigma(\gamma\gamma \rightarrow \Lambda\bar{\Lambda})$ and $\sigma(\gamma\gamma \rightarrow \Sigma^0\bar{\Sigma}^0)$ cross-section measurements are compared to the predictions of the quark-diquark model calculation ²⁰. The absolute predictions using the standard distribution amplitude ²⁰ (Standard DA) reproduce well the L3 data, the asymptotic DA and the DZ-DA models ²⁰ are excluded. The CLEO ¹⁹ and L3 ¹⁸ $\sigma(\gamma\gamma \rightarrow \Lambda\bar{\Lambda})$ cross-section measurements and L3 $\sigma(\gamma\gamma \rightarrow \Sigma^0\bar{\Sigma}^0)$ cross-section measurements for $W > 2.5$ GeV are satisfactorily described also by the handbag model, see Ref. ¹³.

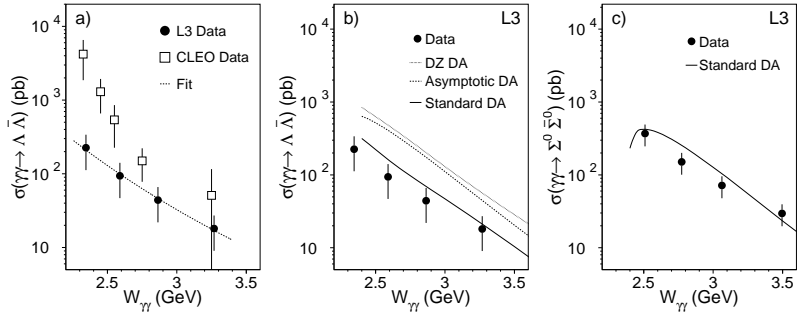


Figure 4. Measurements of the $\sigma(\gamma\gamma \rightarrow \Lambda\bar{\Lambda})$ and $\sigma(\gamma\gamma \rightarrow \Sigma^0\bar{\Sigma}^0)$ cross-sections as a function of W . In a) the $\sigma(\gamma\gamma \rightarrow \Lambda\bar{\Lambda})$ cross-section is compared to the one obtained by CLEO ¹⁹. The dashed line shows the power law fit as described in the text. In b) and c) the $\sigma(\gamma\gamma \rightarrow \Lambda\bar{\Lambda})$ and $\sigma(\gamma\gamma \rightarrow \Sigma^0\bar{\Sigma}^0)$ measurements are compared to the quark-diquark model predictions ²⁰

References

1. G.P. Lepage and S.J. Brodsky, Phys. Rev. **D22** 2157 (1980).
2. G.R. Farrar, E. Maina and F. Neri, Nucl. Phys. **B259** 702 (1985).
3. V.L. Chernyak and I.R. Zhitnitsky, Nucl. Phys. **B246** 52 (1984).
4. ARGUS Collaboration, H. Albrecht et al., Z. Phys. **C42** 543 (1989).
5. CLEO Collaboration, M. Artuso et al., Phys. Rev. **D50** 5484 (1994).
6. VENUS Collaboration, H. Hamasaki et al., Phys. Lett. **B407** 185 (1997).
7. OPAL Collaboration, G. Abbiendi et al., Eur. Phys. J. **C28** 45 (2003).
8. L3 Collaboration, P. Achard et al., Phys. Lett. **B571** 11 (2003).
9. BELLE Collaboration, Chen-Cheng Kuo et al., Phys. Lett. **B621** 41 (2005).
10. C.F. Berger and W. Schweiger, Eur. Phys. J. **C28** 249 (2003).
11. M. Anselmino, F. Caruso, P. Kroll and W. Schweiger, Int. J. Mod. Phys. **A4** 5213 (1989).
12. P. Kroll, M. Schürmann and W. Schweiger, Int. J. Mod. Phys. **A6** 4107 (1991).
13. M. Diehl, P. Kroll and G. Vogt, Eur. Phys. J. **C26** 567 (2003).
14. G. A. Schuler, Comp. Phys. Comm. **108** 279 (1998).
15. S.J. Brodsky and G.R. Farrar, Phys. Rev. Lett. **31** 1153 (1973).
16. V.A. Matveev, R.M. Muradian and A.N. Tavkhelidze, Nuovo Cim. Lett. **7** 719 (1973).
17. V.M. Budnev, I.F. Ginzburg, G.V. Meledin and V.G. Serbo, Phys. Rep. **15** 181 (1974).
18. L3 Collaboration, P. Achard et al., Phys. Lett. **B536** 24 (2002).
19. CLEO Collaboration, S. Anderson et al., Phys. Rev. **D56** 2485 (1997).
20. C.F. Berger and W. Schweiger, Eur. Phys. J. **C39** 173 (2005).